JOURNAL OF GEOPHYSICAL RESEARCH, VOL. 91, NO. A4, PAGES 4381–4392, APRIL 1, 1986

Generation of Band–Limited VLF Noise Using the Siple Transmitter: A Model for Magnetospheric Hiss

R. A. HELLIWELL, D. L. CARPENTER, U. S. INAN, AND J. P. KATSUFRAKIS

Space, Telecommunications, and Radioscience Laboratory, Stanford University, California

Band-limited VLF noise generated by the experimental transmitter at Siple Station, Antarctica, is used to simulate the interaction of natural magnetospheric hiss with energetic radiation belt particles. While the observed spectrum of the generated noise at times closely resembles that of natural VLF hiss, at other times discrete emissions are found to be generated from the incoherent noise signal. Results imply that magnetospheric chorus can be triggered by hiss signals, indicating the similarity of generation mechanisms for coherent and incoherent VLF emissions. A model based on second-order cyclotron resonance can explain the conversion of the relatively short duration wavelets of a hiss spectrum into the longer, semicoherent discrete emissions that are typical of chorus.

1. INTRODUCTION

Very low frequency chorus and hiss are well known forms of electromagnetic emissions that arise in the magnetosphere. However, their origins are poorly understood. Chorus and hiss signals are believed to play an important role in the precipitation of electrons from the radiation belts [*Kennel and Petschek*, 1966; *Foster and Rosenberg*, 1976; *Helliwell et al.*, 1980*a*; *Chang and Inan*, 1983]. Understanding the generation mechanisms of such emissions is clearly important to plasma physics and to the building of models of radiation belts in the earth's magnetosphere and elsewhere in the cosmos.

This paper describes an experimental simulation of magnetospheric hiss in the outer plasmasphere, using the VLF transmitter at Siple Station, Antarctica. Figure 1 shows schematically a magnetospheric propagation path connecting Siple and the conjugate station at Roberval, Quebec. The purpose of the experiment was to better understand the connection between mid-latitude "hiss" [*Dowden*, 1971; *Ondoh et al.*, 1981] and the discrete narrow-band emissions that are known collectively as "chorus." In addressing mid-latitude hiss phenomena, we specifically exclude plasmaspheric hiss, which is generally seen only on satellites [*Muzzio and Angerami*, 1972; *Thorne et al.*, 1973], and auroral VLF hiss, which is associated with the aurorae and may extend to much higher frequencies [*Ellis*, 1957; *Jorgensen*, 1966].

Results of the experiments reported in this paper indicate that spectral elements of the simulated hiss can, under favorable conditions, link together to form chains of choruslike emissions. We suggest therefore that both hiss and chorus could be generated by the coherent wave instability that is found to be excited by signals from the Siple transmitter [*Helliwell and Inan*, 1982; *Helliwell*, 1983].

Mid-latitude hiss and chorus, as observed on the ground and in satellites, often appear together in the same frequency band [*Helliwell*, 1965; *Burtis and Helliwell*, 1976; *Koons*, 1981]. Hiss emissions observed on the ground can develop from a train of whistler echoes [*Helliwell*, 1965] and are on occasion associated with periodic emissions and power line radiation [*Helliwell et al.*, 1975]. Beyond the plasmapause, emission activity as observed on satellites appears to be largely spontaneous in origin (i.e., no triggering source can be identified), although on occasion triggering by whistlers has been observed [*Smith et al.*, 1985]. Satellite observations show that apparently spontaneous, discrete emissions may arise within bands of hiss [*Burtis and Helliwell*, 1976; *Koons*, 1981]. These features of hiss and chorus support the proposed hypothesis linking hiss and chorus to the same basic mechanism.

Paper number 5A8826.
0148-0227/86/005A-8826$05.00

2. EXPERIMENT DESCRIPTION

Magnetospheric hiss may be approximated by band-limited white noise, that is, noise whose power spectral density is constant over a given frequency band. We note, however, that a flat power spectrum imposes only minimal restrictions on the possible time domain sample functions of the noise. As an example, sample functions of the noise power spectrum of band-limited thermal noise can exhibit wide fluctuations in amplitude. Thus, one possible way of generating band-limited noise is to use a thermal noise generator and filter its output over the desired frequency range for transmission. This technique was not employed here because the Siple transmitter is peak-power-limited, and the average transmitted power would then be much less than the peak power of the transmitter. Average signal powers close to the peak transmitter power capability are usually needed, since temporal growth and triggering have been found to occur only above a threshold transmitter power [*Helliwell et al.*, 1980*b*]. This threshold, while variable in time, has typically been close to the peak power available. Our solution to this problem was to generate band-limited noise by modulating only the frequency of the carrier. A crude approximation to a white noise spectrum was considered adequate at this time since the statistical properties of natural hiss have not yet been measured.

In the present experiment the frequency of the carrier was changed every 10 ms to the next value in a list of 100 frequencies randomly selected within a chosen bandwidth. The phase was continuous at each frequency step. The same sequence of 100 frequencies was repeated every second. It can be shown that the power spectral density of such a randomly frequency modulated carrier is very nearly

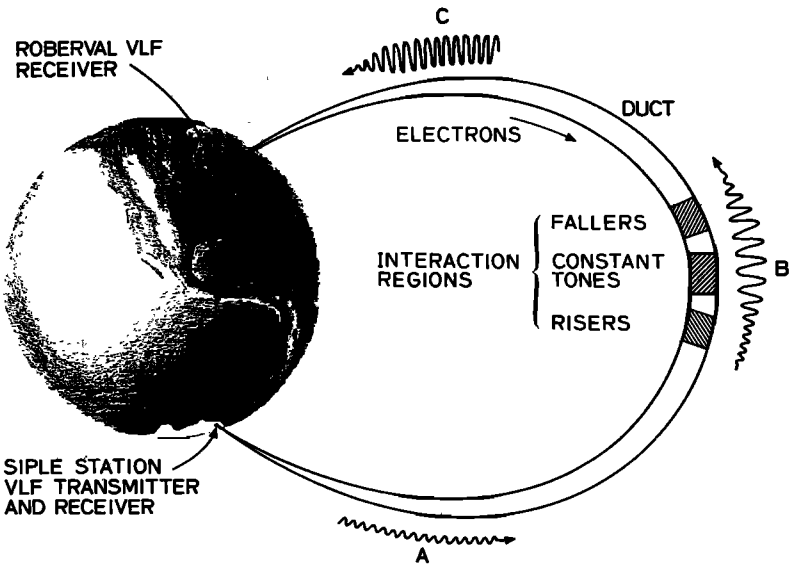

Fig. 1. Schematic of ducted VLF propagation and wave growth between Siple Station and Roberval, Quebec.

flat over the selected bandwidth (W_a), as long as the elementary pulse length T is a few times larger than $(2/W_a)$ [*Papoulis*, 1984]. While the time domain function for such a signal is clearly different from that of, for example, thermal noise, dispersion on the magnetospheric path would be expected to alter the relative times of arrival of the 10-ms wave trains. At the equatorial plane the result is a variable amplitude spectrum that is likely to be a better approximation of band-limited random noise than is the transmitted pattern since the former would also exhibit amplitude fluctuations.

The range of carrier frequencies was chosen to resemble natural hiss as closely as possible without exceeding the bandwidth of the antenna, ~ 400 Hz. Figure 2 shows Roberval $f - t$ spectrograms from experiments in which the noise bandwidth was varied over the range 0–400 Hz. At the left in both panels is the final ~ 2 s of a simulated hiss transmission with bandwidth 400 Hz, centered at 2.36 kHz, as indicated in Figure 2*a* by an arrow. Following on both panels are 5-s simulated hiss transmissions centered at 2.56 and 2.16 kHz (arrows at right in Figure 2*a*). In each transmission the hiss bandwidth was stepped at 1-s intervals over the range 100 Hz to 0 Hz, as shown below Figure 2*b*. The output signal and the rate of triggering were found to increase inversely with the bandwidth. Little difference was seen between 100 Hz and 400 Hz bandwidth. Accordingly, 400 Hz was adopted as a satisfactory compromise. Shorter elementary pulse lengths, of 2 ms and 5 ms, were also used, but appeared not to produce significant growth effects. This is to be expected, since for $T \leq 5$ ms, the condition $2/W_a < T$ cannot be satisfied while at the same time keeping the signal bandwidth within the selected bandwidth of 400 Hz. In other words, for very short pulses the spectrum necessarily extends beyond W_a, and hence the spectral density is reduced. With a reduction in the effective intensity, the input signals are less likely to exceed the threshold for growth and triggering.

Spectra of the hiss as transmitted are shown for analyzer filter bandwidths of $\Delta f = 40$ Hz and 20 Hz, respectively, in the top two panels of Figure 3. With $\Delta f = 40$ Hz, the time sequence of the 10-ms hiss elements is well defined, but the frequency resolution is not sufficient. With $\Delta f = 20$ Hz, the time resolution is not quite enough to resolve the pulse length but frequency resolution is better. In this case two pulses with about the same carrier frequencies, spaced by 10 ms, show a boxlike pattern that reveals lines spaced ~ 50 Hz apart, close to the frequency resolution of the 20-Hz filter. As a compromise $\Delta f = 20$ Hz was used for most routine analysis of the cases discussed in this paper.

The degree to which the artificially generated hiss can be viewed as an approximation to natural hiss is illustrated in Figure 4. The transmitted format is shown in Figure 4*a*, while Figures 4*b* and 4*c* show the simulated hiss as received at Roberval. These are compared with band-limited white noise derived from a laboratory generator (Figure 4*d*) and with samples of natural hiss observed at Roberval (Figure 4*e*). The spectra show that all three samples of noise have similar "speckle" patterns. The experimentally simulated hiss seems to be reasonably consistent with natural magnetospheric hiss and laboratory hiss, at least in terms of the dynamic power spectra shown in Figure 4.

3. RESULTS

In this section we present the experimental results, after a brief discussion of the whistler mode propagation path analysis.

Path Analysis

Because of dispersion, the time delays of individual wave elements vary with frequency. In Figure 3 the transmitted format is aligned with the corresponding 10-ms pulses at the lower edge of the noise spectrum received at Roberval. Unfortunately, in some other cases such as those of Figure 4, alteration of the received pattern, due either to multipath propagation or emission triggering, masks the correspondence between the transmitted and received element patterns. In such cases the beginning and end of the transmissions were used for group time delay measurements, and confirmed with analysis of whistlers observed near the time of the experiment.

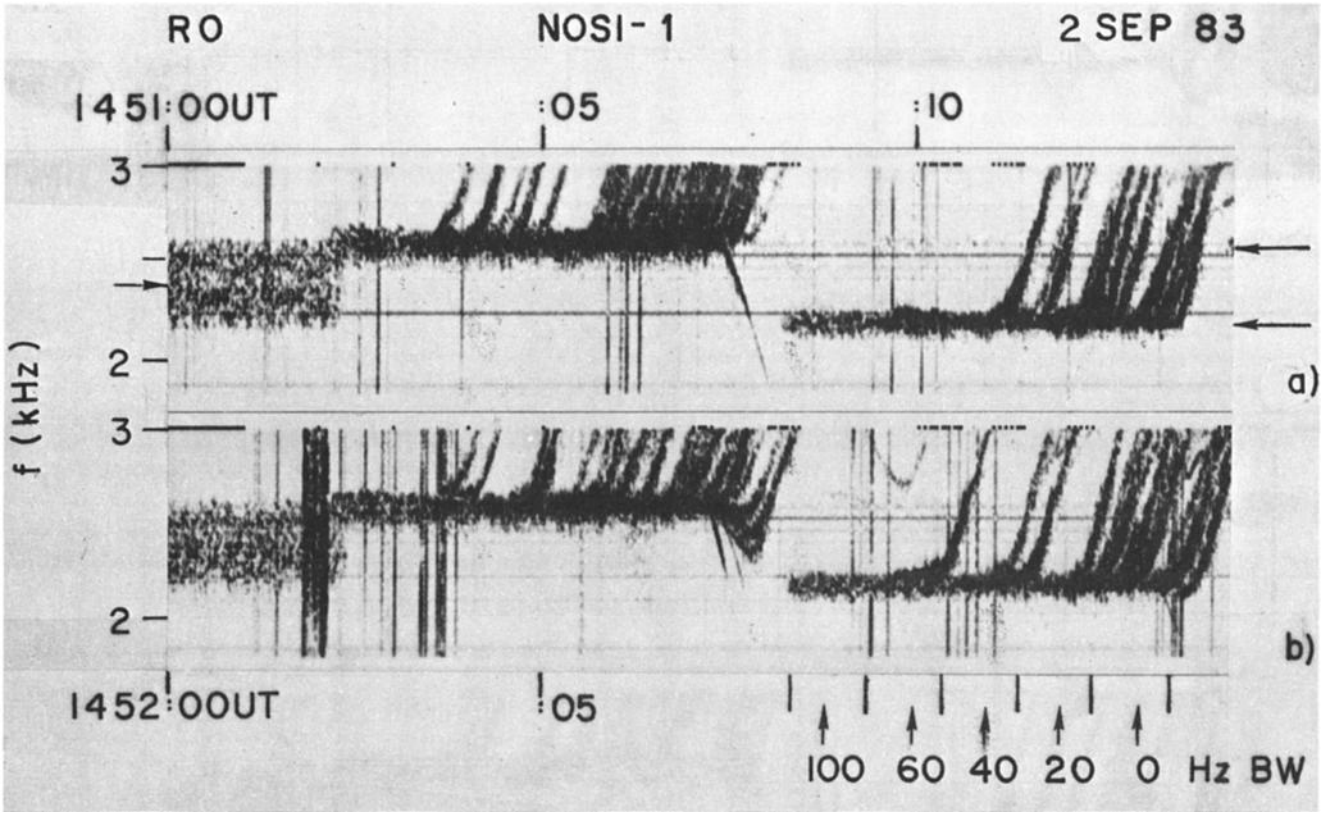

Fig. 2. Response to five contiguous 1-s pulses of simulated hiss, with 100, 60, 40, 20 and 0 Hz bandwidth. At left of record are the last 2-s of the 400-Hz band of simulated hiss. The total intensities at 400 Hz and 100 Hz are roughly the same, but from 100 Hz to 0 Hz the average intensity rises about 10 dB.

In one case, shown in Figure 3, the time shift of the hiss pattern was readily determined. The times of arrival for selected 10-ms pulses were found to be in good agreement with the dispersion of a nose whistler recorded at Roberval at 1620 UT. The results showed a nose frequency of 3.4 kHz, corresponding to a path located at $L = 4.6$. The one-hop delay at the whistler nose frequency was 2.29 s, corresponding to an equatorial electron density of 170 el/cc. For a typical model of the distribution of the cold background plasma along the field lines, the differential phase shift as observed at the equator between two transmitted wave trains of frequency difference Δf is estimated to exceed π radians for $\Delta f \geq 2$ Hz. Thus dispersion causes the phase shift to be essentially random for most pairs of hiss elements.

The differential group delay causes some elements to overlap and others to be separated in time. Two completely overlapping 10-ms elements with a frequency spacing exceeding 100 Hz would interfere constructively at some point during their period of overlap, causing the peak received intensity to be doubled ($\sim$ 6 dB) with respect to that of a single element. In the less likely circumstance where three overlapping elements have the same phase at their centers, the peak intensity would triple, corresponding to a $\sim$ 9.5-dB increase. The amplitude record in the bottom panel of Figure 3 shows a range of amplitude fluctuations of roughly 5–7 dB in the absence of any significant structure on the dynamic spectrum. This is consistent with the frequent overlap of two hiss elements. However, when discrete emissions are present in the received hiss spectrum this range can increase to $\sim$ 12 dB, which can be accounted for by a gain of $\sim$ 5 dB.

Hiss-Chorus Connection

Figure 3c shows several examples of the formation of choruslike emissions from the individual 10-ms wavelets of the simulated hiss. Two of the stronger discrete emissions are labeled *A* and *B* and repeat each second with only slight changes in spectral shape. The amplitude of the entire band of hiss is shown in Figure 3*d*. In both the spectra and the amplitude records the 1-s repetition period of the received hiss pattern is clearly evident. The only nonrepetitive components are the atmospheric "spikes," three examples of which are labeled '*s*' on Figure 3*d*.

The origins of chorus emissions *A* and *B* in Figure 3 can be seen by comparing the transmitted element pattern (Figures 3*a* and 3*b*) with the received pattern of Figure 3*c*. In each case, the chorus emission follows a rising sequence of four successive 10-ms hiss elements, shown by arrows in Figures 3*a* and 3*b*. Each emission was found to reach its peak amplitude (~ -20 dB) near the end of the second element. The amplitude remains constant for $\sim$ 70 ms in case *A* and 50 ms in case *B*. The durations of the unbroken emission traces, as measured from the data of Figure 3*c*, are $\sim$ 115 ms and $\sim$ 80 ms for *A* and *B*, respectively. In case A the emission develops into a falling tone, extending $\sim$ 60 ms beyond the last transmitted hiss element. It terminates at the next line of elements, possibly due to suppression by the overlapping signals [*Helliwell*, 1983].

From Figure 3*d* we see that the maximum intensity of chorus emissions marked *A* and *B* is $\sim$ 6 dB above the average level. From these results we conclude that the individual

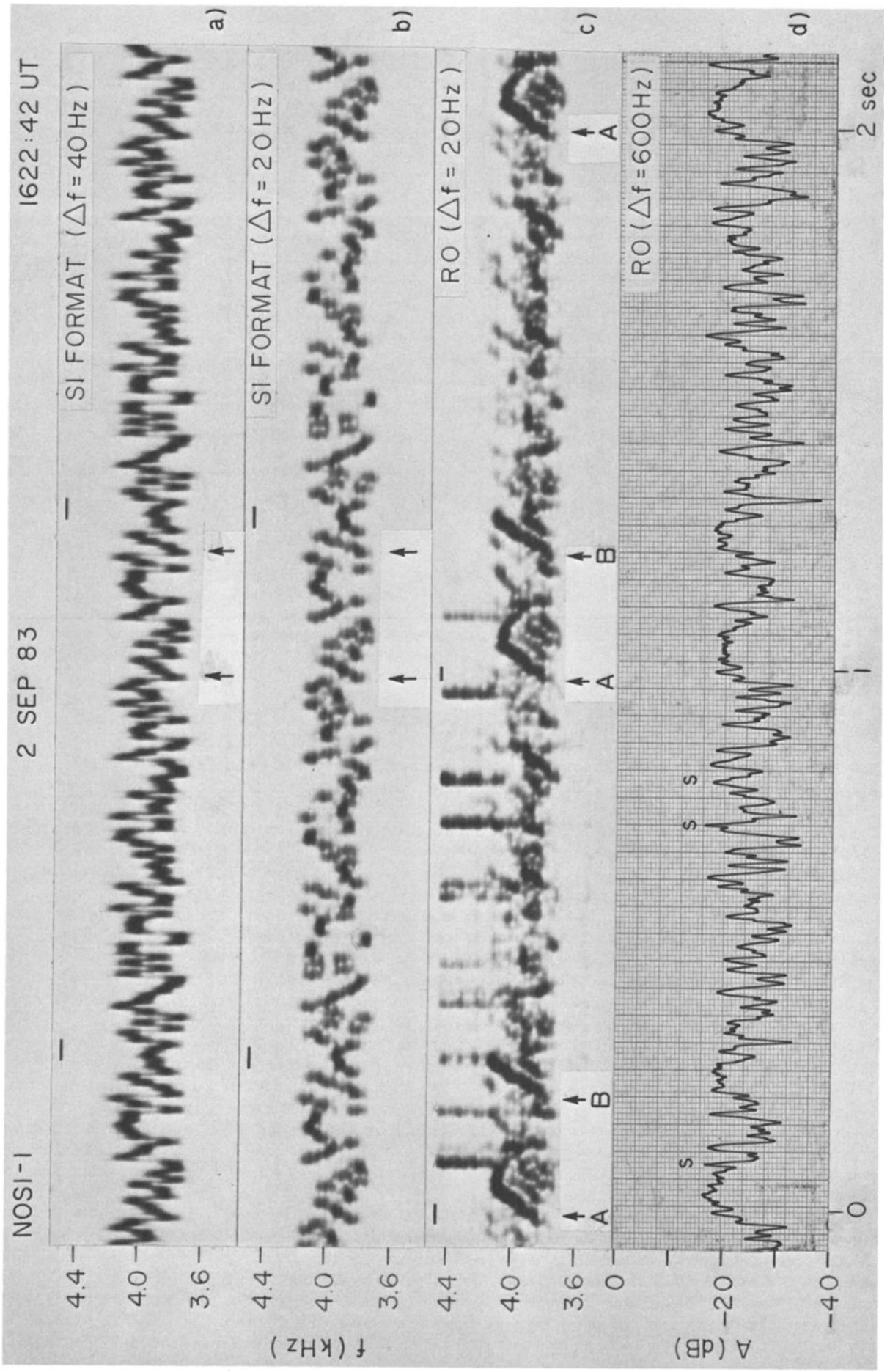

Fig. 3. (*a*) Transmitted spectrum with 40-Hz filter. (*b*) Same as Figure 3*a* except with 20-Hz filter. (*c*) Received spectrum, aligned in time at lower frequency of hiss band. Many individual elements can be associated between Figures 3*b* and 3*c*, revealing a relative delay of the upper edge with respect to the lower of ~ 30 ms. (*d*) Wideband amplitude of hiss band, Figure 3*c*, using a 150-Hz low-pass filter in the output of the detector.

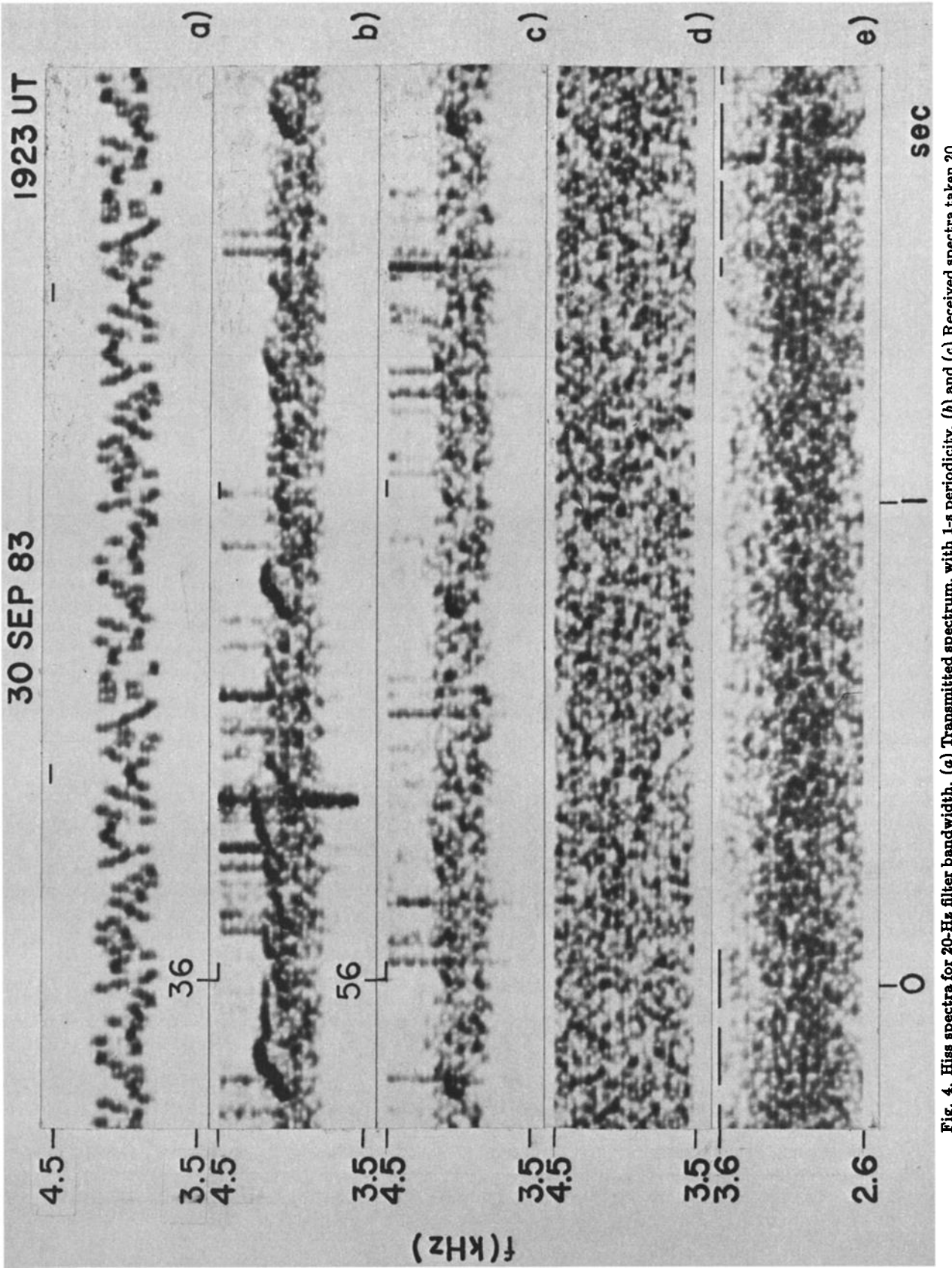

Fig. 4. Hiss spectra for 20-Hz filter bandwidth. (*a*) Transmitted spectrum, with 1-s periodicity. (*b*) and (*c*) Received spectra taken 20 s apart showing changes and similarities in 1-s pattern. (*d*) Spectrum of hiss from a laboratory random noise generator. (*e*) Spectrum of natural hiss received at Roberval on February 14, 1977 at 1216 UT.

input elements act together to amplify and control the (f,t) curve of the emission. In essence, the 10-ms wave trains form quasi-coherent chains that produce enhanced and extended emissions resembling chorus.

The favorable phasing that is postulated to give rise to the formation of the discrete emissions A and B would be expected to change with temporal variation of dispersion over the propagation path. An example is shown in Figure 4 in which two simulated hiss segments spaced 20 s apart are compared in Figures 4*b* and 4*c*. Although the 1-s periodicity of chorus elements is evident, only a remnant of one emission in Figure 4*b* is visible in Figure 4*c*. Other examples, not shown, confirm that discrete emission elements, such as A and B, usually do show significant repeatability from one second to the next. However it is also true that over a period of many seconds discrete emissions may appear in new locations in the pattern, suggesting that the particular phasing of the signals from the transmitter is not the primary cause of the generation of emissions. Such temporal changes in the location of emissions can be attributed to altered phasing among the input wavelets as the path length changes due for example to duct drifts [*Carpenter and Seely*, 1976].

Hiss-Triggered Emissions

A prominent feature of natural hiss is its tendency to trigger free-running emissions at the upper edge of its band [*Helliwell*, 1965]. Similar phenomena have also been observed in the hiss simulation experiment.

In one case shown in Figure 2, the signal power output was held constant while the bandwidth was initially reduced from 400 Hz to 100 Hz and then progressively reduced in 1-s steps from 400 Hz to 0 Hz in 5-s. At 400 and 100 Hz there was no triggering and the rms output was the same. As the bandwidth was reduced from 100 Hz to 0 Hz, the average intensity increased by $\sim$ 10 dB. Rising emissions were triggered for bandwidths less than $\sim$ 60 Hz. The frequency of triggering increased as the bandwidth was reduced. Falling emissions were triggered only when the transmitted signal was terminated at the end of each 5-s segment. There was some tendency for the pattern of triggered emissions to repeat from one 5-s segment to the next. We interpret these results to mean that below an overall bandwidth of 100 Hz, there are enough small steps in Δf to significantly enhance the correlation of phase between some wavelets, in spite of dispersion. Above 100 Hz, on the other hand, dispersion effectively randomizes most of the phase shifts between successive wave trains, so that the signal more closely resembles random noise when it reaches the equator.

In another case, shown with the transmitter format in Figure 5*a*, a 20-s-long, 400-Hz-wide hiss band triggered risers near the top of the band. The riser pattern showed a 1-s periodicity, with a triggering rate of about three risers per second. This periodicity demonstrates that triggering was synchronized by the transmitted hiss signal. Figure 5*b* shows an experiment conducted 30 s later, in which the frequency sequence of the 10-ms hiss elements in the hiss band was inverted with respect to the center frequency by simply reversing the sign of each frequency change with respect to the center frequency. The triggering rate and periodicity are similar; however, the times of triggering in each 1-s segment are clearly different, probably due to the different element pattern near the upper edge of the band.

This experiment demonstrates that free-running triggered emissions can arise in hiss in the absence of coherent triggering signals. The predominance of rising (rather than falling) emissions may be understood by considering second-order cyclotron resonance [*Helliwell*, 1970; *Carlson et al.*, 1985]. In this model risers are generated on the downstream side of the equator, while fallers are generated on the upstream side, as shown schematically in Figure 1. Since the waves propagate opposite to the flow of cyclotron-resonant electrons, the risers cross the equator and pass through the faller generation region. Fallers, on the other hand, must travel away from the equator and hence can never encounter the riser generation region. Thus risers can preferentially suppress the generation of fallers, while fallers cannot influence the generation of risers.

The threshold for triggering of chorus emissions by hiss is found by varying the rms amplitude of the simulated hiss. The results are shown in Figure 6, in which the input signal amplitude is first increased (Figure 6*a*) and then decreased (Figure 6*b*) with time in steps of 2 dB every 2 s. Triggering occurs only for input signals within 4 dB of peak power. Thus emission triggering by hiss is sensitive to both bandwidth and amplitude, just as in the case of emission triggering by coherent signals.

Hiss Plus Coherent Signal

Natural hiss frequently coexists and interacts with nearly monochromatic wave components, such as magnetospheric line radiation and VLF signals from ground sources. An example, Figure 7, shows natural hiss at Roberval gradually building up in strength, along with fixed lines that are believed to be generated by the Canadian power grid [*Helliwell et al.*, 1975]. Multiphase periodic emissions begin building up at $\sim$ 1.3 min, with each emission tending to start at one of these fixed lines. For example, the line at $\sim$ 2.8 kHz in the last half of the third panel from the top is host to a periodic emission with a two-hop emission period of $\sim$ 4.7 s. Because of dispersion the repetition period of the emission depends on the starting frequency, causing the overall pattern of components to change slowly with time. It can be postulated that the superposition of the hiss with a line occasionally enhances the probability of triggering, and such emissions may echo and themselves combine with the same or different lines to initiate more emissions. In this way a complex periodic structure can be created.

A test of the above hypothesis is shown in Figure 8*a*, where a continuous wave signal is added to a 400-Hz artificial hiss band, having a 1-s periodicity. Both signal components have the same rms intensity. The transmitted signal, the received dynamic spectrum and the broadband amplitude are shown respectively in Figures 8*a*, 8*b*, and 8*c*. Emissions, predominantly risers, are triggered sporadically starting at $\sim$ 3.8 kHz. While at first glance the pattern looks irregular, there are features in the emission pattern that exhibit a precise 1-s periodicity; one such set is labeled $A_1 \ldots A_8$. Elements A_4 and A_5 are missing, presumably because the input signals were below the triggering threshold at those times. The two sharp terminations of emissions, at 22.35 s and 23.35 s, are exactly 1-s apart, suggesting that the termination of an emission sequence may also be controlled by the relative phasing of the hiss elements. Variation in this

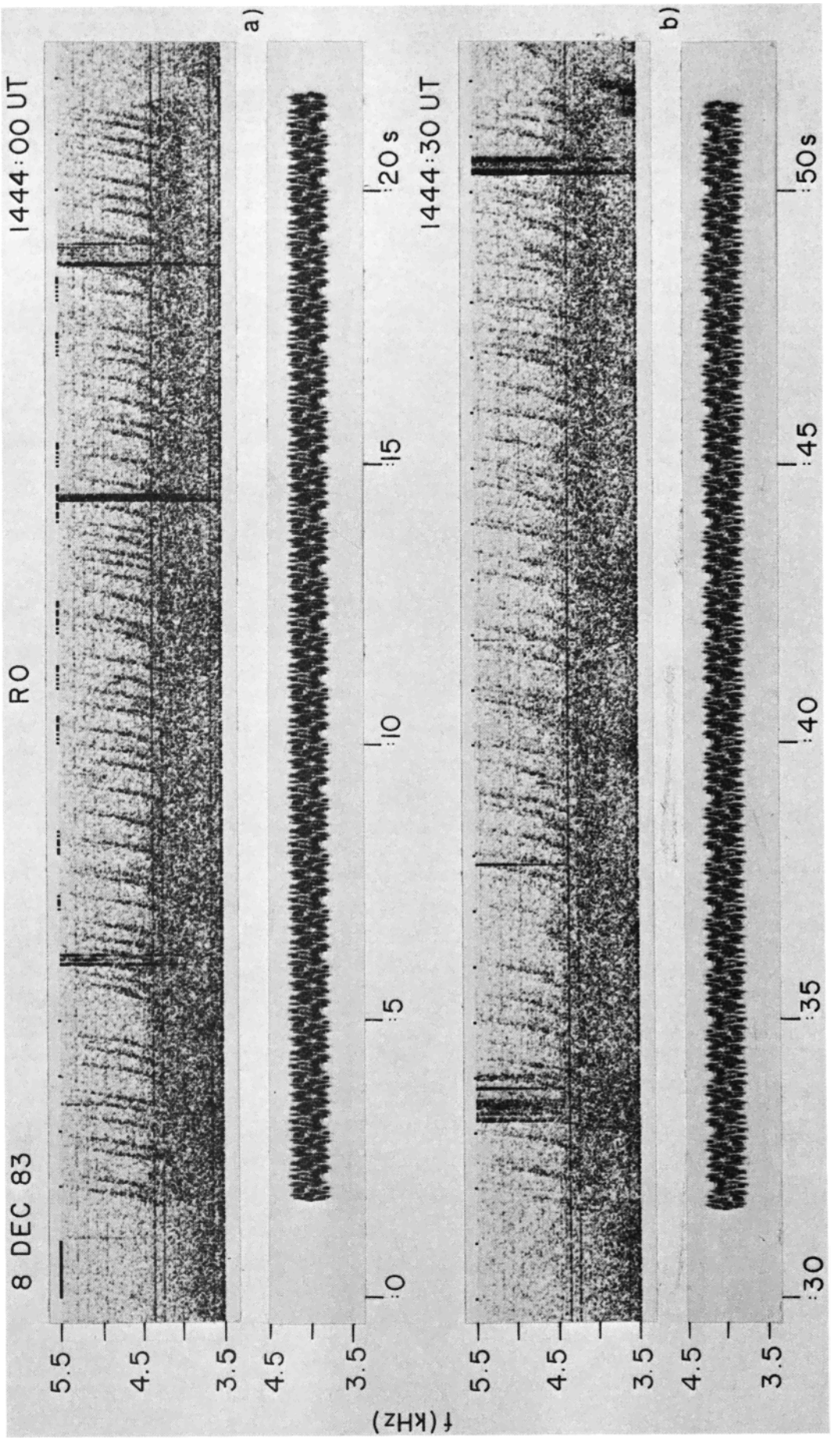

Fig. 5. (a) 400-Hz hiss band triggers chorus with pronounced 1-s periodicity. (b) Same, but with inverted sequence of element frequencies.

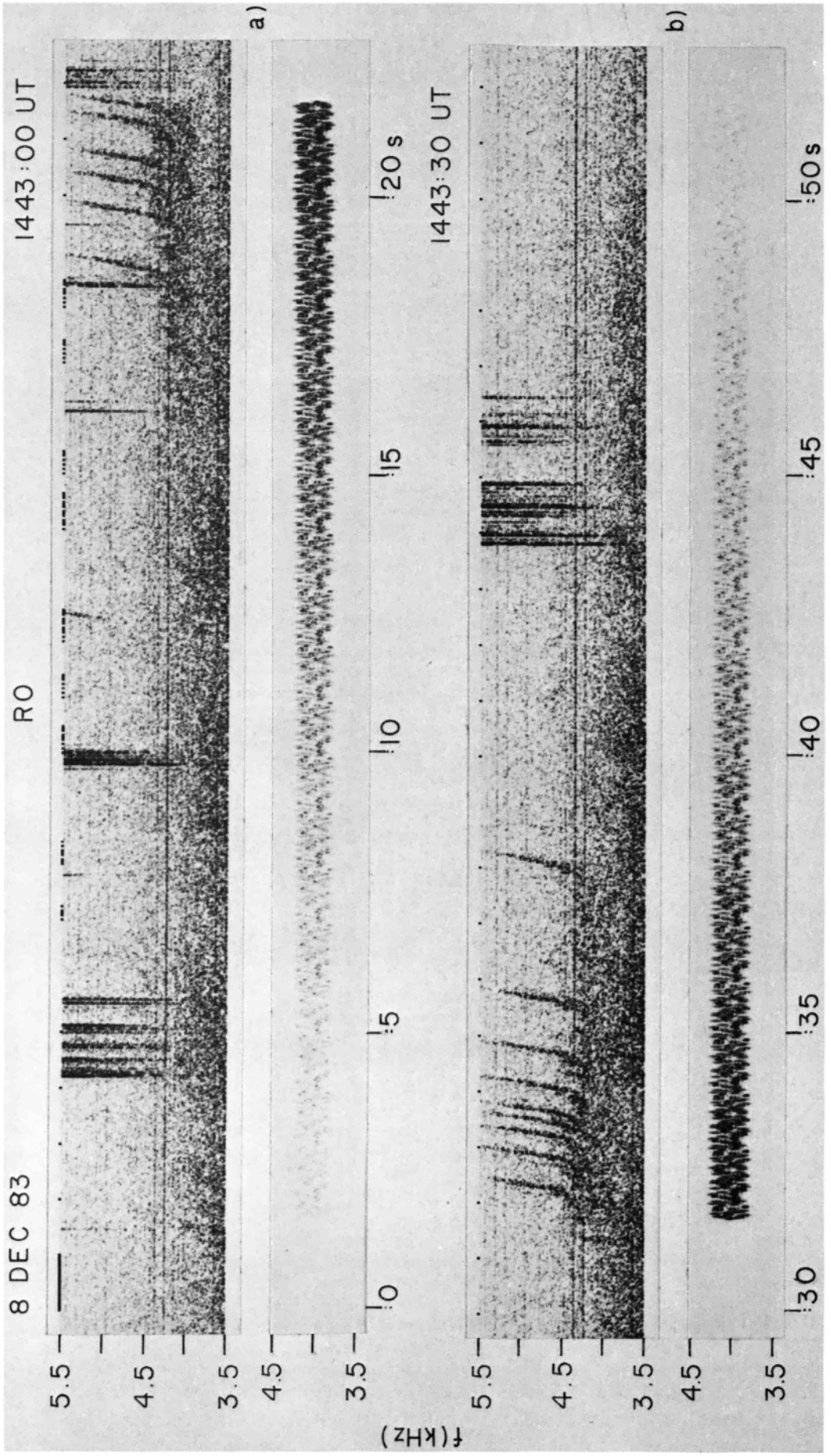

Fig. 6. Transmitted hiss band is stepped in amplitude 2 dB every 2 s, (*a*) up and (*b*) down. Received hiss (upper panel in each case) shows triggering only for amplitude of 0 dB, -2 dB, and -4 dB. Natural hiss is present at lower frequencies.

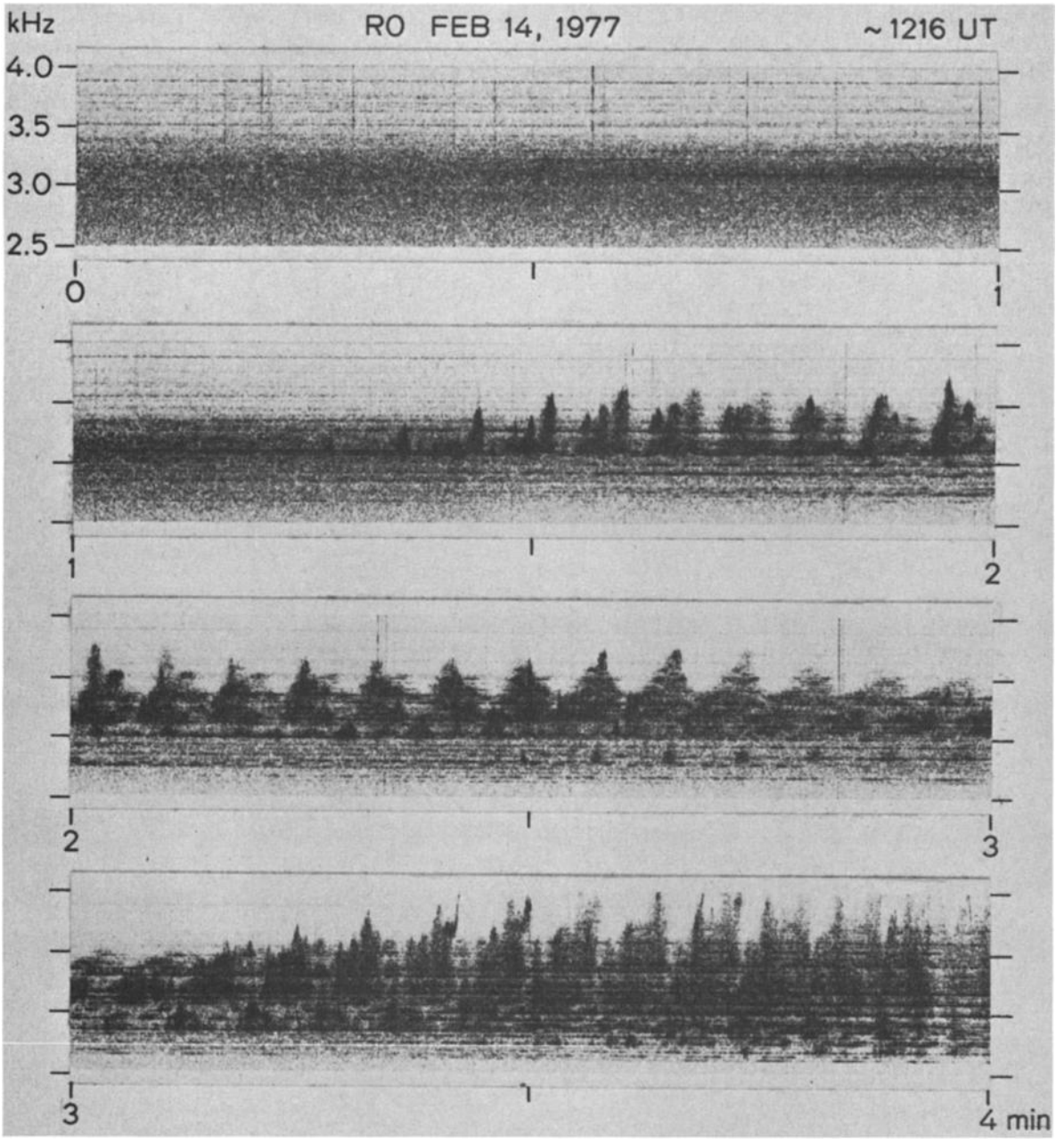

Fig. 7. Natural hiss, power line radiation and periodic emissions observed at Roberval, February 14, 1977.

relation would be expected to occur as a result of temporal changes in the energetic particle flux or duct drift effects.

4. INTERPRETATION

The observed conversion of hiss to chorus can be accounted for by considering second-order cyclotron resonance [*Helliwell*, 1970; *Carlson et al.*, 1985], which occurs when the spatial variation of the Doppler-shifted radiation frequency and the electron gyrofrequency are matched at a point along the field line as determined by the frequency-time slope of the wave. The length of the second-order resonance interaction region, for a linear frequency-time variation, is approximately independent of the slope, as long as the frequency-time slope and particle pitch angles are not too large [*Helliwell*, 1970].

Thus the phase bunching process tends to be qualitatively independent of the frequency-time slope. However as this slope increases, the second-order interaction region moves away from the equator, causing both the electron gyrofrequency and the corresponding electron parallel velocity to increase. Then for typical electron distribution functions, the energetic particle flux and corresponding growth rate fall off, leading to reduced growth and emission activity. This effect becomes noticeable at slopes greater than a few kilohertz per second.

Consider each pair of sequential hiss elements to be equivalent to a signal with an average slope equal to the frequency spacing of the elements divided by the time interval between their centers. To illustrate we use discrete emission B from Figure 3. For simplicity we assume that the time relationships in the actual second-order resonance region are the same as predicted for the equator. Since in this experiment

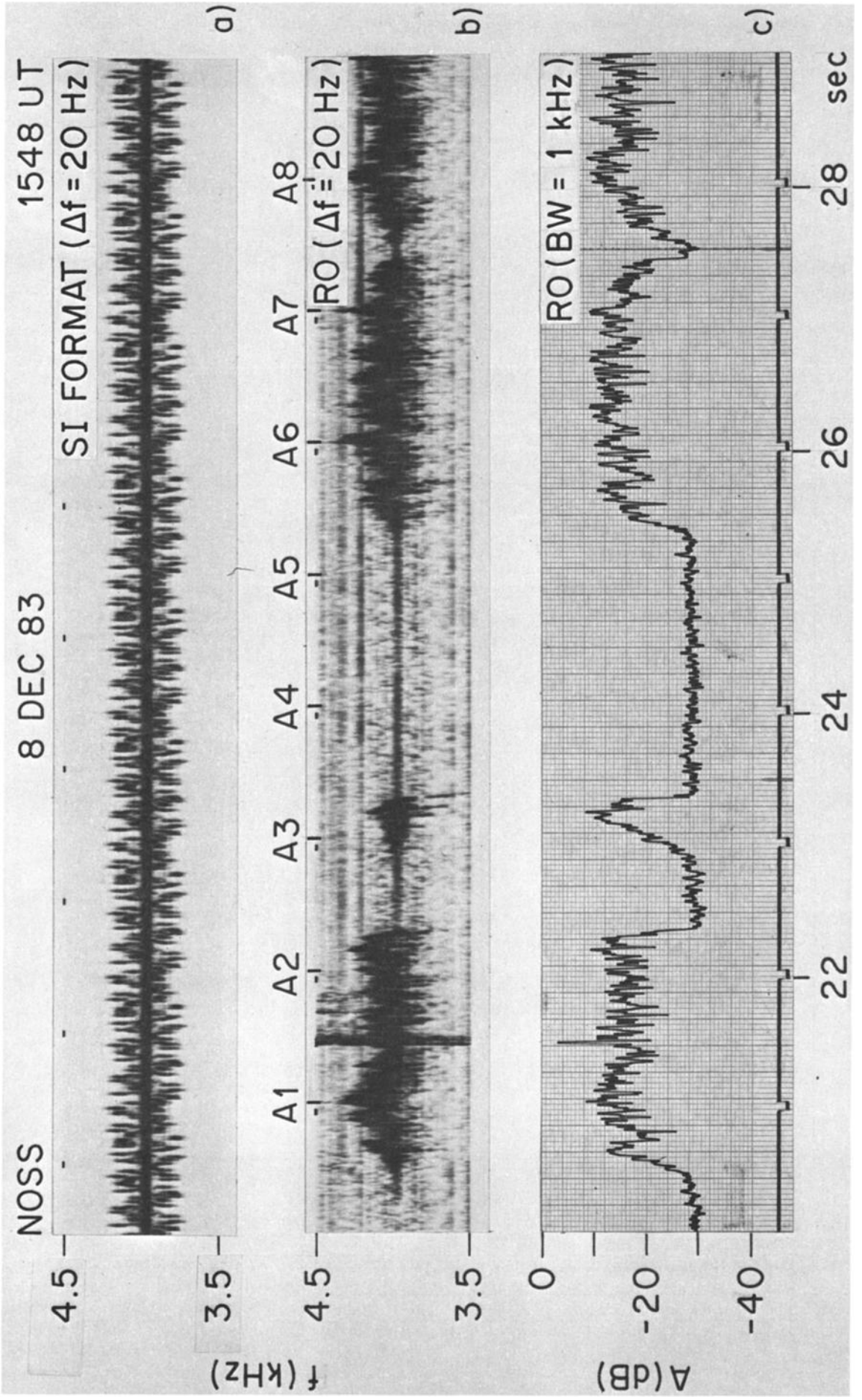

Fig. 8. Simulated hiss plus CW signal at center frequency. (*a*) Format, (*b*) Received spectrum, (*c*) Amplitude of received signal.

all hiss frequencies are above the whistler nose frequency, dispersion causes the group delay to increase with frequency, leading to the appearance of gaps between the elements of emission B as received at Roberval. Gaps are assumed to be filled by emissions that are triggered by the previous element. Coherence requires that the phase of an emission that starts in the first hiss element be matched to the phase of the second element. Since dispersion tends to randomize the relative phase between two elements spaced more than a few hertz, the emission slope must change slightly to achieve proper phasing. Since the phase can never differ by more than π, we need to shift the phase by no more than $\pm\pi$ in the frame of the second element in order to achieve coherence. Thus for a 10-ms pulse, which at 4 kHz contains 40 cycles, a half-wavelength shift is only one eightieth of the pulse length. Hence only a small change in the slope of this emission is required to achieve phase coherence. In effect, any two signal elements will select the location along the field line at which these two elements can be linked together through a second-order resonance emission. For efficient emission generation according to this model it is necessary that the phase of each signal element remain close to that of the sloping emission. Fortunately, certain early experiments at Siple Station employed staircases of 10-ms pulses to represent frequency ramps. Growth rates and total growth were found to show little variation with slope for slopes less than a few kilohertz per second [*Helliwell and Katsufrakis*, 1978].

To assess this point quantitatively, we will assume that the signal phase must be within $\pi/4$ of the ideal ramp function in order to preserve phase coherence. Further, we assume that the ideal ramp passes through the center of the 10-ms pulse. The maximum phase shift between the ramp and the pulse is then given by

$$\phi = \int_0^{T/2} \Delta\omega\, dt = 2\pi \int_0^{T/2} \frac{df}{dt} t\, dt = \frac{\pi}{4}\left(\frac{df}{dt}\right) T^2 \text{ rad}$$

where T is pulse length in seconds and df/dt is slope in hertz per second. For $\phi = \pi/4$, the maximum allowable slope for a 10-ms pulse is given by

$$\frac{df}{dt}\Big|_{\max} = 10\,\text{kHz/s}$$

Since the slopes of emissions A and B of Figure 3, corrected for the one-half-hop dispersion from equator to receiver, are less than this limit, we conclude, subject to our assumptions, that a sequence of 10-ms constant-frequency elements is an adequate approximation to a signal with continuously varying frequency.

For typical coherent wave growth rates of 120 dB/s a pair of 10-ms pulses would give $\sim$ 2.4-dB growth, not enough to account for the $\sim$ 6 dB rise, above the average, of events A and B in Figure 3. However if the third element would happen to have nearly the same phase as the amplified output of elements 1 and 2, the result would be a $\sim$ 40-ms-long effective ramp, and then the corresponding growth would be $\sim$ 6 dB, as required.

The above assumption of the required phase coherence ($\pi/4$) is somewhat arbitrary. A full theory of the interaction is needed in order to test this assumption. In the meantime, the particular mechanism that is suggested here can serve as a working hypothesis to stimulate both theoretical modeling and further experiments.

5. Discussion and Conclusions

Chorus and mid-latitude hiss are closely associated observationally, as many past experiments have shown. Results shown in this paper demonstrate that sequential simulated hiss elements alone can, under favorable conditions, be transformed into discrete chorus emissions, or even fully developed triggered emissions. Our conclusions must be tempered with the realization that although the dynamic spectra of the man-made hiss and natural hiss are similar (Figure 4), such spectra do not fully describe the time domain characteristics of the signal. Until better simulations of noise are available, our experiment should be understood to support, rather than confirm, the hypothesis that chorus and mid-latitude hiss are generated by the same basic mechanism.

Wave-wave suppression can account for the prevalence of rising versus falling emissions and the tendency of risers to start at the upper edge of a hiss band. Falling tone emissions would be expected to be generated on the upstream side of the equator [*Helliwell*, 1967] and would tend to be suppressed by adjacent rising emissions that would have been generated earlier on the downstream side (see Figure 1). Likewise, risers that start below the upper edge of a band of echoing hiss must pass through various hiss elements before emerging into the relatively quiet range above the hiss band. Thus only those risers triggered near the upper edge of the hiss band can develop with little interference.

Finally we note the interesting implications of the result shown in Figure 6, illustrating that the maximum transmitter power output is only a few decibels above the threshold for the triggering of emissions by hiss elements. A substantial increase in effective radiated power, for example 5–10 dB, should enlarge the opportunities for active experiments on wave-particle interactions involving "incoherent" signals in the magnetosphere. The problem is a fundamental one, since much of the intense VLF noise from natural plasmas is hisslike in character. From a theoretical point of view, the marriage of hiss and chorus would generate conceptual offspring that could aid the development of a more comprehensive theory of wave growth and emission triggering in the magnetosphere.

Acknowledgments. We acknowledge useful discussions with our colleagues at the STAR Laboratory and the contributions of Dave Shafer as the winter-over science leader at Siple Station during 1983. The spectra shown were processed by J. Yarborough, and whistler data analysis was aided by C. Williams. The manuscript was typed by G. Walker. This research was supported by the Division of Polar Programs of the National Science Foundation under contracts DPP-83-17092 and DPP-83-18508.

The Editor thanks H. C. Koons and R. L. Dowden for their assistance in evaluating this paper.

References

Burtis, W. J., and R. A. Helliwell, Magnetospheric chorus: Occurrence patterns and normalized frequency, *Planet. Space Sci.*, *24*, 1007, 1976.

Carlson, C. R., R. A. Helliwell, and D. L. Carpenter, Variable frequency VLF signals in the magnetosphere: Associated phenomena and plasma diagnostics, *J. Geophys. Res.*, *90*, 1507, 1985.

Carpenter, D. L., and N. T. Seely, Cross-L plasma drifts in the outer plasmasphere: Quiet time patterns and some substorm effects, *J. Geophys. Res.*, *81*, 2728, 1976.

Chang, H. C., and U. S., Inan, Quasi-relativistic electron precipitation due to interactions with coherent VLF waves in the magnetosphere, *J. Geophys. Res.*, *88*, 318, 1983.

Dowden, R. L., Distinctions between mid latitude VLF hiss and discrete emissions, *Planet. Space Sci., 19*, 374, 1971.

Ellis, G. R., Low-frequency radio emission from aurorae, *J. Atmos. Terr. Phys., 10*, 303, 1957.

Foster, J. C., and T. J. Rosenberg, Electron precipitation and VLF emissions associated with cyclotron resonance interactions near the plasmapause, *J. Geophys. Res., 81*, 2183, 1976.

Helliwell, R. A., *Whistlers and Related Ionospheric Phenomena*, Stanford University Press, Stanford, Calif., 1965.

Helliwell, R. A., A theory of discrete VLF emissions from the magnetosphere, *J. Geophys. Res., 72*, 4773, 1967.

Helliwell, R. A., Intensity of discrete VLF emissions, in *Particles and Fields in the Magnetosphere*, edited by B. M. McCormac, p. 292, Reidel, Dordrecht, Holland, 1970.

Helliwell, R. A., Controlled stimulation of VLF emissions from Siple Station, Antarctica, *Radio Sci., 18*, 801, 1983.

Helliwell, R. A., and U. S. Inan, VLF wave growth and discrete emission triggering in the magnetosphere: A feedback model, *J. Geophys. Res., 87*, 3537, 1982.

Helliwell, R. A., and J. P. Katsufrakis, Controlled wave-particle interaction experiments, in *Upper Atmosphere Research in Antarctica, Antarctic Res. Ser.*, Vol. 29, pp. 100–129, AGU, Washington, D. C., edited by L. J. Lanzerotti and C. G. Park, 1978.

Helliwell, R. A., J. P. Katsufrakis, T. F. Bell, and R. Raghuram, VLF line radiation in the earth's magnetosphere and its association with power system radiation, *J. Geophys. Res., 80*, 4249, 1975.

Helliwell, R. A., S. B. Mende, J. H. Doolittle, W. C. Armstrong, and D. L. Carpenter, Correlations between λ4278 optical emissions and VLF wave events observed at $L \sim 4$ in the Antarctic, *J. Geophys. Res., 85*, 3376, 1980*a*.

Helliwell, R. A., D. L. Carpenter, and T. R. Miller, Power threshold for growth of coherent VLF signals in the magnetosphere, *J. Geophys. Res., 85*, 3360, 1980*b*.

Jorgensen, T. S., Morphology of VLF hiss zones and their correlation with particle precipitation events, *J. Geophys. Res., 71*, 1367, 1966.

Kennel, C. F., and H. E. Petschek, Limit on stably trapped particle fluxes, *J. Geophys. Res., 71*, 1, 1966.

Koons, H. C., The role of hiss in magnetospheric chorus emissions, *J. Geophys. Res., 86*, 6745, 1981.

Muzzio, J. L. R., and J. J. Angerami, Ogo 4 observations of extremely low frequency hiss, *J. Geophys. Res., 77*, 1157, 1972.

Ondoh, T., Y. Nakamura, S. Watanabe, and T. Murakami, Narrow-band 5 kHz observed in the vicinity of the plasmapause, *Planet. Space Sci., 29*, 65, 1981.

Papoulis, A., *Probability, Random Variables and Stochastic Processes*, McGraw-Hill, New York, 1984.

Smith, A. J., D. L. Carpenter, and U. S. Inan, Whistler-triggered VLF noise bursts observed on the DE-1 satellite and simultaneously at Antarctic ground stations, *Ann. Geophys., 3*, 81, 1985.

Thorne, R. M., E. J. Smith, R. K. Burton, and R. E. Holzer, Plasmaspheric hiss, *J. Geophys. Res., 78*, 1581, 1973.

D. L. Carpenter, R. A. Helliwell, U. S. Inan, and J. P. Katsufrakis, Space, Telecommunications, and Radioscience Laboratory, Stanford University, Stanford, CA 94305.

(Received August 8, 1985;
revised November 18, 1985;
accepted November 25, 1985.)